
A KNEE CANNOT HAVE LUNG DISEASE: OUT-OF-DISTRIBUTION DETECTION WITH IN-DISTRIBUTION VOTING USING THE MEDICAL EXAMPLE OF CHEST X-RAY CLASSIFICATION

A PREPRINT

Alessandro Wollek^{*,2}, Theresa Willem^{3,4}, Michael Ingrisch⁵, Bastian Sabel⁵ and Tobias Lasser^{1,2}

¹Munich Institute of Biomedical Engineering, Technical University of Munich

²Department of Informatics, Technical University of Munich

³Institute for History and Ethics in Medicine, Technical University of Munich

⁴Munich School of Technology in Society, Technical University of Munich

⁵Department of Radiology, University Hospital, Ludwig-Maximilians-Universität

August 3, 2022

Keywords out-of-distribution detection, chest x-ray classification, outlier detection, anomaly detection

ABSTRACT

Deep learning models are being applied to more and more use cases with astonishing success stories, but how do they perform in the real world? To test a model, a specific cleaned data set is assembled. However, when deployed in the real world, the model will face unexpected, out-of-distribution (OOD) data. In this work, we show that the so-called “radiologist-level” CheXnet model fails to recognize all OOD images and classifies them as having lung disease. To address this issue, we propose in-distribution voting, a novel method to classify out-of-distribution images for multi-label classification. Using independent class-wise in-distribution (ID) predictors trained on ID and OOD data we achieve, on average, 99 % ID classification specificity and 98 % sensitivity, improving the end-to-end performance significantly compared to previous works on the chest X-ray 14 data set. Our method surpasses other output-based OOD detectors even when trained solely with ImageNet as OOD data and tested with X-ray OOD images.

1 Introduction

Modern machine learning models are achieving great successes in real world medical applications, such as diabetic retinopathy diagnosis Gulshan et al. [2016], skin cancer classification Esteva et al. [2017], or lung disease assessment Rajpurkar et al. [2017, 2018a], Majkowska et al. [2019]. Due to the early and profound digitization of imaging techniques, machine learning in radiology can already show convincing successes, such as the detection of certain critical pathologies of the lung on X-ray images non-inferior to radiologists Rajpurkar et al. [2017]. Considering the increasing demand for imaging while the number of radiologists remains insufficient, such and similar models can help improve medical patient care Ali et al. [2015], Idowu and Okedere [2020], Rosman et al. [2015], Rosenkrantz et al. [2016], Rimmer [2017], e.g., by screening acquired radiographs for critical findings prior to radiologist interpretation. Then, patients with time sensitive illnesses will receive treatment earlier, potentially saving their lives.

What all of these chest X-ray classifiers have seen, once trained, validated and tested, are chest X-rays of a certain type, the in-distribution (ID) images. Consequently, the features learned depend on the assumption that the input is ID. But despite the advanced level of digitization, individual workflows for creating and archiving radiological images and linking them to other patient data are subject to manual intervention by staff and are consequently prone to human error, breaking this assumption. Just one example would be that mixed-up labelling arises of patients for

*alessandro.wollek@tum.de

whom X-ray images of several body parts have been taken. Consequently, images of a knee joint, for example, would be fed to a model for detecting pulmonary pathologies. Hence, in the aforementioned example, the presentation of out-of-distribution (OOD) images, erroneous and potentially patient-harming events are possible.

A major problem of current deep learning models is that they make high confidence predictions when facing unexpected, OOD, data Nguyen et al. [2015], Nalisnick et al. [2019], Hendrycks et al. [2021], like a knee X-ray. In our example, prioritization based on false, high-confidence, OOD X-rays can lead to longer waiting times for other patients with time critical conditions, like a pneumothorax, potentially risking their life until the error is discovered and resolved. Moreover, repeated instances of such misreporting will - if not balanced with transparency measures sufficiently - quickly lead physicians to distrust the model, eventually leading them refrain of using it [Robinette et al., 2017, Vayena et al., 2018, Nov et al., 2021].

Therefore, in recent years, several methods Hendrycks and Gimpel [2017], Hendrycks et al. [2020], Wang et al. [2021], Hendrycks et al. [2019] have been proposed to detect OOD samples. Commonly, the OOD detector converts the output of a model to an ID probability. For example, Max. Probability Hendrycks et al. [2020] uses the highest class probability as ID probability. Another approach, proposed by Lee et al. Lee et al. [2018] models OOD based on the the smallest Mahalanobis distance between the input and a class conditional Gaussian distribution in the latent space.

So far, the problem caused by OOD data has been investigated only on toy data sets, e.g. a model trained on the CIFAR-10 data set Krizhevsky and Hinton [2009], learning to classify automobiles and trucks, is tested on the SVHN data set Netzer et al. [2011] containing house numbers. This raises the question if the test performance of proposed OOD detectors translate to an existing model trained on chest X-rays. Figure 1 motivates this problem: as the real world data consists of more than frontal chest X-rays a classifier like CheXnet Rajpurkar et al. [2017] must handle OOD images safely.

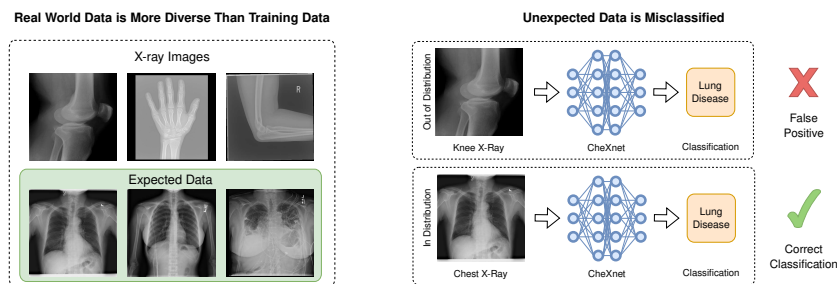


Figure 1: Deep learning models in the real world must be able to handle OOD data. **(left)** A chest X-ray classifier (CheXnet) is trained on chest X-rays and tested with expected production data: chest X-rays. In a clinic, the model has to handle non chest X-ray images confidently, as the data cannot be manually cleaned beforehand. **(right)** A model trained and tested only on chest X-ray images will incorrectly classify OOD images (here: an X-ray of a knee) as having lung disease.

In this work, we are addressing the practical consequences of OOD data by examining the impact of non chest radiographs on the so-called “radiologist-level” chest X-ray classifier CheXnet. The major contributions of our work are: we systematically explore the OOD detection performance of the CheXnet chest X-ray classifier on three realistic OOD data sets; we show that the benchmark performance of current OOD detection methods mostly do not translate to this domain; and we demonstrate that our proposed method in-distribution voting (IDV) improves OOD detection and generalizes to other data sets.

2 Results

CheXnet We investigate the effect of X-ray OOD data on the performance of an existing, “radiologist-level” chest X-ray classifier. We trained the CheXnet model Rajpurkar et al. [2017] on the Chest X-ray 14 (CX_R14) data set Wang et al. [2017]. The data set consists of 112,120 frontal chest radiographs with 14 annotated chest pathologies (see Figure 3 c for a list of labels). The model achieved a mean area the under the receiver operating characteristic curve (AUC) of 83 % when tested without OOD images, as shown in Table Appendix 3.

As an image might display signs of multiple pathologies, classifying these images is modeled as a multi-label classification task, where each class is predicted independently. Images that do not show any signs of these 14 diseases are labeled as “no finding”, which has been modeled as not predicting any of the 14 classes. The consequence is that OOD

predictions are indistinguishable from “no finding” predictions, as the CheXnet model must predict zero probability for all 14 classes in both cases.

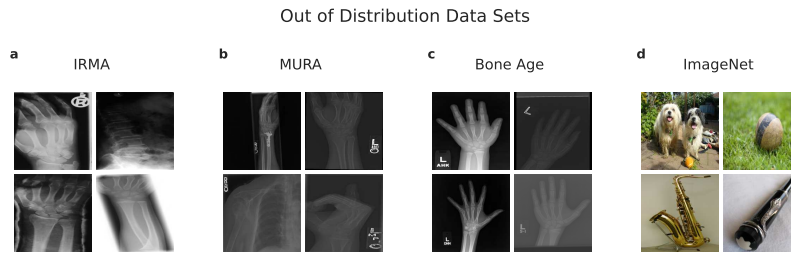


Figure 2: Out-of-distribution data sets used in this work. We used three radiographic data sets (IRMA Deserno and Ott [2009] (a), MURA Rajpurkar et al. [2018b] (b), and BoneAge Halabi et al. [2019] (c)) and the ImageNet Russakovsky et al. [2015] (d) data set. The IRMA data set is a diverse radiographic data set. The MURA data set contains only upper extremity radiographs. The Bone Age data set consists of hand radiographs. The ImageNet data set contains web scraped photographs. All data sets are publicly available.

OOD Data Sets Not every OOD sample is equally likely in a real-world scenario. The CheXnet model can encounter OOD X-ray images, as the distinction between ID and OOD X-ray images is based on manual, error-prone, tagging. Photographs on the other hand are not part of the image processing pipeline in a radiology department and can thus be assumed not to be found in a real-world scenario. For our experiments, we selected three publicly available radiographic data sets, IRMA Deserno and Ott [2009], MURA Rajpurkar et al. [2018b], and BoneAge Halabi et al. [2019], containing images of various body parts as realistic OOD test data sets to test cross-data set generalization Torralba and Efros [2011]. While the CheXnet model has been pre-trained on predicting the ImageNet classes, they are OOD regarding the target task of chest X-ray classification, as the data set does not include chest X-rays. Therefore, we use it as additional non chest X-ray OOD data set, allowing us to investigate the performance of our proposed method “In-Distribution Voting” (IDV) when trained with a large-scale unrealistic OOD data set. This is relevant for use cases where no or only few realistic OOD images are available. The OOD data sets are illustrated in Figure 2:

- **IRMA**: the image retrieval in medical applications data set Deserno and Ott [2009] consists of 14,410 diverse radiographic images; 12,677 are annotated according to the anatomical category, 1733 are test images without annotation.
- **MURA**: the musculoskeletal radiographs data set Rajpurkar et al. [2018b] consists of 40,561 radiographic images, displaying different upper extremity bones.
- **BoneAge**: the Bone Age data set Halabi et al. [2019] consists of 12,811 hand radiographs of children.
- **ImageNet**: the ImageNet data set Russakovsky et al. [2015] contains over one million web scraped photographs. The data set is often used for pre-training computer vision models.

We specifically chose publicly available data sets to ensure reproducibility of our findings, and selected multiple OOD data sets to test how the different OOD detection methods generalize to images from various sources. Further data set details are listed in Table 1 and described in Section 5.1. Our corresponding code is available at <https://gitlab.lrz.de/IP/a-knee-cannot-have-lung-disease>.

To investigate the effect of OOD images on the CheXnet predictions we measured how many OOD images are incorrectly classified as ID, i.e. the model predicts the presence of a disease while there is none. Here we found, that the standard CheXnet model fails to reject any OOD image across all three test data sets, achieving an ID specificity of 0 % on all three X-ray OOD test data sets, as shown in Figure 3 a. These results provide evidence that the model’s prediction is (unsurprisingly) conditioned on the assumption that the input image is a chest X-ray image. An acclaimed “radiologist-level” model that cannot distinguish between a chest and a knee will be experienced as unreliable and untrustworthy by physicians and therefore potentially not used at all. The ID sensitivity is 97.8 % although the model’s prediction of “no finding” ID and OOD images are indistinguishable. Accounting for it by removing “no finding” samples increases the sensitivity from 97.8 % to 99.7 %, as shown in Figure 3 b.

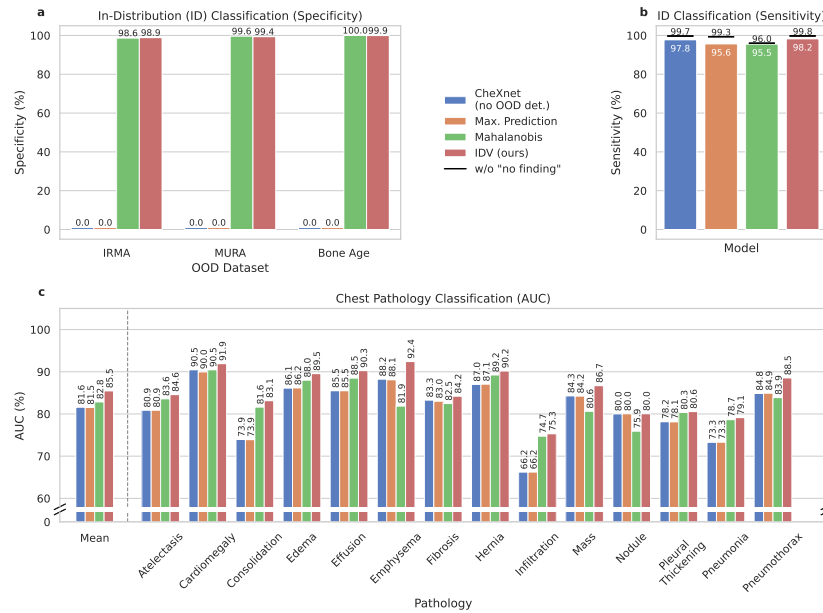


Figure 3: Effect of OOD images on OOD detection and end-to-end model performances. **(a)** CheXnet Rajpurkar et al. [2017] misclassifies nearly all OOD images as chest X-ray images (specificity 0 %). Adding an output-based OOD detector like Max. Prediction Hendrycks et al. [2020] to the trained model did not improve the specificity. The activation-based Mahalanobis OOD detector Lee et al. [2018] improved the specificity to 99 % - 100 % across the three X-ray OOD data sets. Our proposed method, In-Distribution Voting (IDV), trained with additional IRMA and ImageNet OOD images performed equally with a specificity of 99 % - 100 % across the three X-ray OOD data sets. **(b)** Accounting for CheXnet’s incapability to differentiate between “no finding” and OOD by removing “no finding” samples increases the sensitivity from 97.8 % to 99.7 %. While Max. Prediction did not improve the sensitivity (95.6 %, 99.3 % without “no finding” samples) and specificity it allows to differentiate between “no finding” and OOD. Mahalanobis performed similarly with a sensitivity of 95.5 %. Removing “no finding” samples increases the sensitivity barely (96 %). IDV increases CheXnet’s ID sensitivity to 98.2 %, 99.8 % without “no finding” samples. **(c)** OOD detection using IDV improves downstream chest X-ray classification. Max Prediction’s lower ID sensitivity compared to the vanilla CheXnet model results in a slightly lower average AUC. Mahalanobis’ strong OOD detection did not improve chest X-ray classification for all classes, achieving a lower AUC for emphysema, fibrosis, mass, nodule, and pneumothorax compared to the baseline CheXnet model. IDV performed best, improving the AUC across all classes the most.

OOD Detection Several OOD detection methods have been proposed to predict an ID probability explicitly. Hendrycks and Gimpel were one of the first to address this problem Hendrycks and Gimpel [2017]. They used the maximum value of the softmax prediction as ID probability (**Max. Softmax**). In their work, they motivate this choice by observing that the highest prediction is lower for OOD samples than ID samples. As the softmax is commonly used for single-label classification problems, they extended the method to multi-label classification problems by taking the maximum prediction of the sigmoid (**Max. Prediction**) Hendrycks et al. [2020]. Alternatively, they propose to use the maximum of the underlying logits, the input to the sigmoid layer (**Max. Logit**). Wang et al. use the label-wise energy function Liang et al. [2018] instead of the sigmoid to transform the output of the model to an ID probability score (**Max. Energy**) Wang et al. [2021].

In the OOD literature, the OOD detection performance is typically reported using the threshold independent area under the receiver operating curve (AUC) on an OOD data set Hendrycks and Gimpel [2017], Hendrycks et al. [2019], Wang et al. [2021]. However, without specifying a threshold and reporting the OOD performance on a held-out test data set, the reported results do not answer how these methods would perform in a real-world scenario. Similar to Lee et al. we pick the OOD threshold at an ID classification sensitivity of 95 % Lee et al. [2018]. In contrast to previous works, we do so on the *validation* set (CXR14 + OOD) and report the performance on the test set. This allows us to measure the chest X-ray classification performance in a more realistic scenario: after removing predicted OOD samples on the test set, as shown in Figure 3 c.

We tested several state-of-the-art OOD detection methods (Max. Softmax Max. Energy, Max. Prediction and Max. Logit) to improve the ID classification performance compared to the baseline CheXnet model. Throughout our OOD experiments we use Max. Prediction representatively for the other methods, as they are all output-based and performed similarly (see Table Appendix 2 for a detailed comparison). We found that all methods failed to detect OOD images, as seen in Figure 3 a: the specificity is 0 %. Although predicting the ID probability enables the differentiation of “no finding” ID and OOD images, the ID sensitivity is only 95.6 % compared to 97.8 % without OOD detection (see Figure 3 b). Removing “no finding” samples increases the ID sensitivity to 99.3 %. Due to the lower ID classification performance, the end-to-end performance compared to the CheXnet model is marginally lower (81.6 % AUC without OOD compared to 81.5 % AUC with Max. Prediction), as seen in Figure 3 c.

Instead of converting the model’s output to an ID prediction Lee et al. use the activations of the model to generate class-conditional Gaussian distributions Lee et al. [2018] (**Mahalanobis**). Doing so, they model OOD images as unlikely activations, i.e. having a large Mahalanobis distance to the modeled class means. They motivate using the Mahalanobis distance between the mean representation of a class and the input in the feature space, instead of performing OOD detection in the label space due to “label overfitting”, i.e. that the model predictions are conditioned on the training labels.

Detecting OOD images using the Mahalanobis distance results in a much higher ID specificity compared to the output-based methods: 98 % - 100 % across the three chest X-ray OOD test data sets with a sensitivity of 95.5 %, as seen in Figure 3 a. Removing “no finding” samples increases the sensitivity barely (96 %). As with the output-based methods, the ID threshold was set to have 95 % sensitivity on the validation set. The strong specificity difference between the output based methods and Mahalanobis provides evidence for the “label overfitting” hypothesis. When measuring the end-to-end performance, i.e. measuring the AUC of the disease predictions after removing predicted OOD images, the results were mixed compared to the baseline CheXnet model: for some classes the model performed better (e.g. consolidation, improvement from 73.9 % to 81.6 %) for others the performance decreased significantly (e.g. emphysema from 88.2 % to 81.9 %). One reason for this could be that this method chooses the highest class-wise distance as OOD score instead of considering all classes.

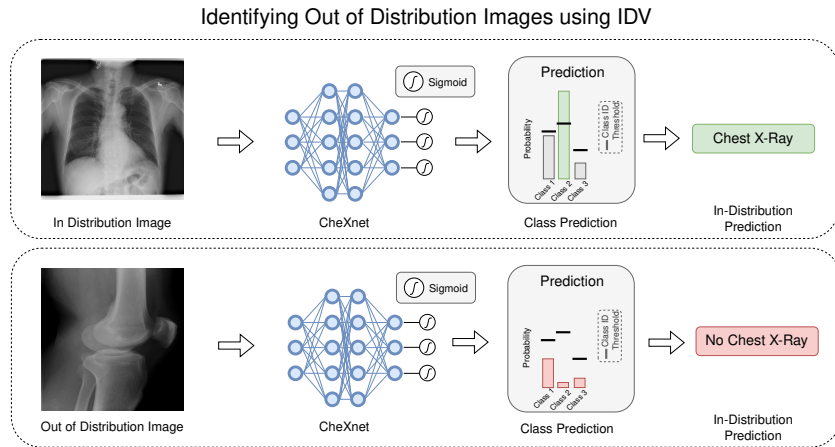


Figure 4: Out-of-distribution (OOD) detection using our proposed method in-distribution voting (IDV). The model is trained with in-distribution (ID) and OOD images. Before inference, class-wise ID thresholds are set to have 95 % sensitivity on the validation set. Only if all classes vote against ID unanimously, a sample is classified as OOD.

In-Distribution Voting To improve the robustness of the model’s prediction and the OOD detection performance we propose In-Distribution Voting (IDV): a sample is classified as ID if at least one class-wise prediction is above the class-wise ID threshold, as illustrated in Figure 4. As the ID threshold is determined using ID and OOD data, we can expect to have some OOD data at hand and leverage it to break the “closed world” assumption during training, i.e. force the model not to condition the prediction on the chest X-ray input assumption. To do so we adapt approaches proposed in the literature Hendrycks et al. [2019], Bevanđić et al. [2019] and include OOD data into the training data set, so called outlier exposure Hendrycks et al. [2019] or negative data Torralba and Efros [2011]. Note, while “no finding” samples have no labeled diseases, we consider them as ID, as they are chest X-rays. The ID thresholds are set for each class independently to have 95 % sensitivity on the validation data set (containing ID and OOD images).

When trained with OOD data from ImageNet and IRMA our method achieves an ID specificity of 98 % - 100 % across the X-ray OOD test data sets while having an ID sensitivity of 98.2 %, as seen in Figure 3 a and b. Removing “no

finding” samples improved the sensitivity further to 99.8 %. Compared to Mahalanobis and the other methods, IDV also improves class-wise end-to-end prediction across all classes (see Figure 3 c) with a mean AUC of 85.5 % compared to the baseline of 81.6 %. The improvement in both sensitivity and specificity compared to other output-based methods like Max. Prediction suggests that training with OOD data strongly improves the model’s OOD detection performance. This is true even when trained with mostly photographs from the ImageNet data set and tested with OOD X-ray images, as seen in Figure 3. We interpret these results as indicating that the model incorporates the fact that OOD images exist into its output. The consistent end-to-end prediction improvements compared to Mahalanobis mixed results demonstrate the importance of querying all classes regarding OOD detection instead of focusing on a single class.

To investigate the effect of training with OOD data on chest disease classification performance we measured the performance on the ID test data set alone, without OOD samples (see Table Appendix 3). We can conclude that training with OOD data, as proposed in our method IDV, does not affect chest disease classification performance. In the subsequent section we analyse how different OOD data sets affect ID classification performance.

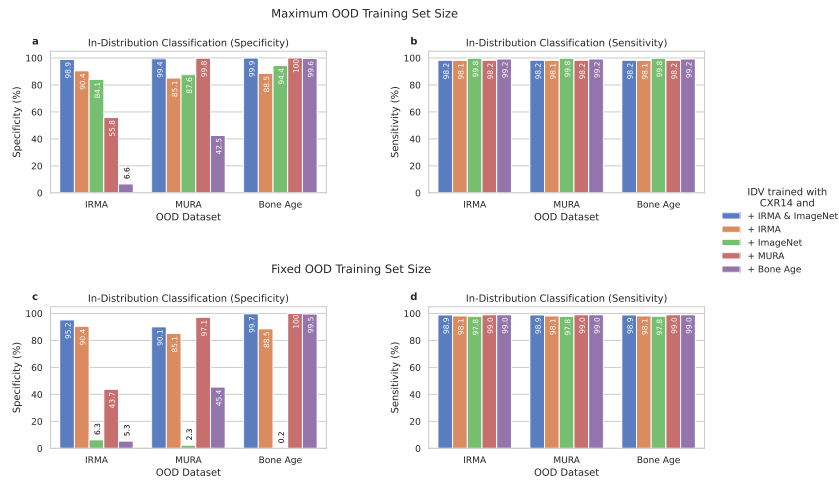


Figure 5: Effect of different OOD training data sets on OOD detection performance across different OOD test data sets. (a) Training with OOD images improves the ID specificity, even when the OOD Images are visually different than the test OOD images (cf. ImageNet). On average, training with a large OOD data set (ImageNet) performs better than training with a small OOD data set. (b, d) All models generalize to the test data, achieving ID sensitivities > 97 %. The ID threshold is set at 95 % validation ID sensitivity. (c) ID specificity is affected by training set size, more strongly when training and test OOD images are from a different data set. IDV trained with ImageNet performance drops by to 0.2 % (Bone Age) when training data is reduced to 3,088 samples, training with IRMA & ImageNet performs best.

Training with OOD Data To investigate the importance of OOD training data set type and size we trained the model with different configurations: with each OOD data set and with each of the OOD data sets limited to the smallest OOD training data set (IRMA, 3088 training images, see Table 1). Furthermore, we trained with ImageNet and IRMA to have both a large OOD data set and diverse OOD X-rays.

We found that training with any OOD data, even the photographs of ImageNet, improved the ID classification specificity compared to the baseline CheXnet model by a large margin, as seen in Figure 5 a. When OOD training and test data stem from the same data set, we see in Figure 5 a that all models achieved an ID specificity of over 98 %. On average, training with ImageNet alone performs better than training with Bone Age. Notably, the ID specificity decreases when tested on OOD data sets that contain more categories than the OOD training data set (e.g. lower extremities in IRMA are not part of MURA, BoneAge contains only hands), highlighting the importance of a diverse OOD data set, except for training with IRMA. Our results suggest that while image diversity has a strong effect on OOD detection, using any OOD data for training, e.g. ImageNet, is an improvement to training without any OOD data. We therefore conclude that using a generic OOD data set alone could improve a model’s OOD detection performance. Including domain specific OOD images improves the ID specificity even further (cf. ImageNet vs. ImageNet + IRMA in Figure 5 a).

Regarding the ID sensitivity, we found no difference across training with chest X-Ray OOD data, as seen in Figure 5 b, d. The ID sensitivity when trained with ImageNet dropped from 99.8 % to 97.2 % when trained with reduced

data (3,088 samples). As the ID classification threshold was determined at 95 % *validation* sensitivity, this shows that all models generalize to the test data.

Accounting for the OOD training data set size (fixing the training set to 3,088 samples) reduces ID specificity, as seen in Figure 5 c. Specifically, we see that reducing the amount of ImageNet training images from 217,818 to 3,088 drastically reduces the OOD detection performance across all OOD test sets, e.g. from 94.4 % to 0.2 % on the Bone Age test data set. Still, training with IRMA and ImageNet achieved a specificity of over 90 % on all data sets, outperforming the model trained with IRMA alone by over 5 %. We conclude, while training the model with OOD images from the test data distribution achieved the highest specificity in general, training with many ImageNet OOD images improved the specificity considerably (from 0 % to 84.1 % - 94.4 %). Furthermore, as application specific OOD samples can be hard to obtain and the sensitivity is affected by OOD training set size, training with a general large OOD data set (ImageNet) and few application specific OOD samples (IRMA) achieves a better performance than training with only a small specific OOD data set.

3 Discussion

Assessing whether the tested model performance in a benchmark translates to an intended production setting, including potential OOD data is a necessary step before deploying a machine learning model. This is particularly important in safety critical applications, e.g. when classifying chest X-rays to assist radiologists in diagnosing patients. Our results show that the so-called “radiologist-level” CheXnet model Rajpurkar et al. [2017] cannot handle OOD samples. A model that cannot handle OOD images, making confident predictions based on wrong evidence, will lead to worse quality of care, eroding the trust of physicians into the model’s predictions when facing ID images, and impede the potential benefits of computer assisted diagnosis.

In this work, we investigated the effect of OOD images on a “radiologist-level” chest X-ray classifier. We showed that the model, reportedly performing as good as radiologists Rajpurkar et al. [2017, 2018a], was not able to filter OOD images, leading to obvious false positives to the human observer. We assume its predictions are conditioned on chest X-rays, because the model was only trained on chest X-rays, leading to overconfident predictions given OOD images. As hypothesised by Lee et al. [Lee et al., 2018], this leads to an ID-overfitted output space. This interpretation explains why established output-based OOD detection methods failed in our experiments, when compared to detecting OOD samples in the feature space. Our solution, ID voting and training with OOD images, regularizes the output space and expands the model’s knowledge horizon, leading to a 100 % ID sensitivity and 98 % specificity.

One reason why OOD data are rarely considered is their dependency on the intended application. We showed that including a small OOD training data set from the same data set as the OOD test data resulted in a higher specificity than a general OOD data set. While this suggests that there is no ideal application independent OOD data set, we found that training with any OOD data improved the baseline performance considerably. Furthermore, we showed that even a few thousand OOD samples from the intended application boosted the specificity considerably. Therefore, when creating a data set to train and evaluate a model in a production setting, we recommend to remove anomalies, outliers and other OOD with caution. Instead, including this “real-world” data not only in the training process, but also into the model validation, will lead to more robust ML models and ultimately improve clinical acceptance

4 Conclusion

In summary, we showed that training only on ID data results in incorrectly classifying all OOD images as ID with the example of chest X-ray classification, resulting in increased false positive rates. We demonstrated, that our method, IDV, improves the model’s ID classification performance substantially even when trained with data that will not occur in the intended use case. Thus, making the final model more robust and improving the predictive performance in a real-world scenario significantly.

5 Methods

5.1 Data Sets

Besides the ID Chest X-ray 14 data set Wang et al. [2017] we used three OOD X-ray data sets (IRMA Deserno and Ott [2009], MURA Rajpurkar et al. [2018b], Bone Age Halabi et al. [2019]) and the ImageNet Russakovsky et al. [2015] data set. The different training, validation, and testing splits are shown in Table 1. All data sets are publicly available.

Data Set	In-	Out-of-Distribution				
	CXR14	IRMA	MURA	Bone Age	ImageNet	Fixed
Pre-processing	-	Remove CXR	-	-	Sample	Sample
Training	78,468	3,088	35,366	8,179	217,818	3,088
Validation	11,219	772	772	772	54,455	772
Testing	22,433	3,860	3,860	3,860	3,860	3,860
Total	112,120	7,720	39,998	12,811	276,133	7,720

Table 1: Data Sets used in our experiments. The smallest out-of-distribution data set (IRMA Deserno and Ott [2009]) is split into 40 %/10 %/50 % training/validation/testing. To compare different scenarios we used the same number of images for validation and testing of the other OOD data sets (MURA Rajpurkar et al. [2018b], BoneAge Halabi et al. [2019], ImageNet Russakovsky et al. [2015]). The remaining images were used for training. Because the ImageNet data set is an order of magnitude larger than the ID CXR14 data set Wang et al. [2017] we took a random sample first. To examine the different data set sizes we also fixed the size of the OOD training data splits to have the same amount of images.

5.1.1 Chest X-ray 14 Data Set

We use the train-test split provided by the authors of the Chest X-ray 14 data set, having non-overlapping patients. We further randomly split the provided training data set into training and validation sets, again with non-overlapping patients resulting in 78,468 training, 11,219 validation, and 22,433 test images (see also Table 1). All three splits have a similar prevalence of class labels. In summary, the original data set is split into 70 % training, 10 % validation, and 20 % test data. We use the images labelled as “no finding” for training, as 46 % of the images are labelled as such. For these images, the model must predict the absence of all 14 pathologies.

5.1.2 Out-of-Distribution Data Sets

Because the IRMA data set is the smallest data set, we sample every OOD data set so that their test and validation split size matches the IRMA splits.

IRMA We only use the provided training images, as we require the IRMA labels to exclude ID chest radiographs from the data set. We remove all chest X-rays from the data set according to their anatomical code and exclude images with an anatomical code starting with 57, 75, 05, or 150, resulting in 7,720 images. We split the remaining images randomly into training, validation, and testing using a 30 % / 20 % / 50 % split to ensure enough images in the test split.

Bone Age We randomly sample the test and validation images according to the data split sizes of the IRMA data set (772 validation images, 3,860 test images, see Table 1). The remaining 8,179 images are used either all or sampled according to the IRMA training set size (3,088 images) for the training split.

MURA We split the MURA data set, containing 40,561 images, similar to the Bone Age data set: the validation and test partitions are randomly sampled, matching the size of the IRMA validation/test splits, listed in Table 1. Either all remaining images or sampled according to the IRMA training set size (3,088 images) are used for training.

ImageNet Due to the size of the ImageNet Large Scale Visual Recognition Challenge (ILSVRC) data set compared to the Chest X-ray 14 data set we use only 50 % of the 544,546 images provided in the “LOC_train_solution.csv” file for training and another 20 % for validation, see Table 1. When accounting for OOD data set sizes, we sample the training and validation sets according to the size of the IRMA splits. For both cases we sample the test set according to the IRMA test split size. All train/validation/test splits were created with non-overlapping images.

5.2 CheXnet

Following [Rajpurkar et al., 2017], we fine-tune a DenseNet-121 Huang et al. [2017] on the CXR14 data set. The model was pre-trained on ImageNet pre-trained and is available on `pytorch.org`. For fine-tuning, we replace the last layer with a fully-connected layer with 14 outputs, matching the 14 classes of the CXR14 data set. The outputs are converted to a probability by applying the sigmoid function. The class-wise predictive thresholds were determined by setting a chest pathology classification sensitivity of 95 % only on the CXR14 validation data set, without any

OOD data. We use binary cross entropy as a loss function and train the model using ADAM Kingma and Ba [2015] optimization with default parameters ($\beta_1 = 0.9$, $\beta_2 = 0.999$) and an initial learning rate of 0.0003. We divide the learning rate by a factor of ten if the validation loss did not improve over the last two epochs. We apply weight decay with a value of 0.0001. We train the model for eight epochs and select the best model based on the validation loss. The input images are resized to 256 x 256 pixels and normalized according to the ImageNet mean and standard deviation. Then we apply 224 x 224 ten crop, i.e., we take crops from each corner and the centre of the image and repeat the process for the horizontally flipped image: producing ten 224 x 224 pixel images per sample. The model predictions of the ten images are averaged before calculating the loss.

Training With Out-of-Distribution Images When including OOD images into the training data, the model must predict the absence of any pathology for the images. Like the ID images, the OOD images are normalised according to the ImageNet mean and standard deviation and passed to the model in the same fashion as the ID images.

5.3 Out-of-Distribution Detection

The goal of OOD detection is to classify each image as either ID or OOD. As a baseline, we used the default CheXnet model. Furthermore, we used Max. Softmax Hendrycks and Gimpel [2017], Max. Energy Wang et al. [2021], Max. Prediction and Max. Logit Hendrycks et al. [2020], and Mahalanobis Lee et al. [2018].

Training with OOD Images When training with OOD images both training and validation splits are extended to include the OOD training/validation splits. For every OOD image, the model must predict the absence of any pathology.

Overall Prediction Classifying OOD images as negative samples due to the absence of any pathology requires a per-class classification threshold. For every pathology we select the ID classification threshold at 95 % ID sensitivity on the validation data set (containing ID and OOD data). If every class-probability for a sample is below the respective threshold the sample is classified as OOD.

Output-Based OOD Detection We convert the model’s 14 class predictions into an ID probability using the highest class-prediction (Max. Softmax Hendrycks and Gimpel [2017] and Max. Prediction Hendrycks et al. [2020]), the highest logit (Max. Logit Hendrycks et al. [2020], Max. Energy Wang et al. [2021]). We select the ID classification threshold at 95 % ID sensitivity on the validation data set (containing ID and OOD data).

Mahalanobis For Mahalanobis-based OOD detection Lee et al. [2018] we use the output of the penultimate layer to determine the Mahalanobis scores. We select the ID classification threshold at 95 % ID sensitivity on the validation data set (containing ID and OOD data).

Declarations

6 Funding

The research for this article received funding from the German federal ministry of health’s program for digital innovations for the improvement of patient-centered care in healthcare [grant agreement no. 2520DAT920].

7 Conflict of interest

The authors report no conflict of interest.

8 Availability of data and materials

All data sets are publicly available. The Chest X-ray 14 data set can be accessed at <https://nihcc.app.box.com/v/ChestXray-NIHCC/>, the IRMA data set at <https://doi.org/10.18154/RWTH-2016-06143>, Bone Age data set at <https://www.rsna.org/education/ai-resources-and-training/ai-image-challenge/rsna-pediatric-bone-age-challenge> and the ImageNet data set at <https://www.kaggle.com/c/imagenet-object-localization-challenge>.

9 Code availability

The code and the trained models are available at <https://gitlab.lrz.de/IP/a-knee-cannot-have-lung-disease>

10 Authors' contributions

AW designed the methodology, implemented the experiments, and carried out the analysis, with contributions of TW, MI, BS, and TL; AW wrote the manuscript with contributions of TW, MI, BS and TL; TL supervised the study.

A Comparison of Output-Based OOD Detectors

	IRMA		MURA		Bone Age	
	Spec.	Sens.	Spec.	Sens.	Spec.	Sens.
Max. Prediction	0 %	95.64 %	0 %	95.64 %	0 %	95.64 %
Max. Softmax	0 %	99.47 %	0 %	99.47 %	0 %	99.47 %
Max. Energy	0 %	95.64 %	0 %	95.64 %	0 %	95.64 %
Max. Logit	0 %	95.79 %	0 %	95.97 %	0 %	95.97 %

Table 2: OOD detection results for output-based OOD methods (Max. Prediction Hendrycks et al. [2020], Max. Softmax Hendrycks and Gimpel [2017], Max. Energy Wang et al. [2021], Max. Logit Hendrycks et al. [2020]) on the IRMA, MURA, and Bone Age test sets. All methods fail to detect the OOD images (Specificity (Spec.) = 0 %) when correctly classifying at least 95 % of the ID, Chest X-ray 14, images (Sensitivity (Sens.) \geq 95 %).

We test several state-of-the-art out-of-distribution detection methods: Max. Softmax Hendrycks and Gimpel [2017], Max. Prediction and Max. Logit Hendrycks et al. [2020], and Max. Energy Wang et al. [2021] on the three OOD test data sets IRMA, MURA and Bone Age. All methods failed to identify the OOD samples, as seen in Table 2.

B Effect of Training With OOD Data on ID Classification

Pathology	CheXnet	OOD Training Data Set				
		IRMA & ImageNet	IRMA	ImageNet	MURA	Bone Age
Atelectasis	0.82	0.82	0.81	0.80	0.82	0.82
Cardiomegaly	0.91	0.91	0.90	0.89	0.90	0.91
Consolidation	0.80	0.80	0.79	0.80	0.81	0.81
Edema	0.88	0.88	0.88	0.86	0.89	0.89
Effusion	0.88	0.88	0.88	0.87	0.88	0.88
Emphysema	0.91	0.91	0.92	0.87	0.92	0.93
Fibrosis	0.82	0.82	0.80	0.78	0.81	0.83
Hernia	0.92	0.88	0.94	0.85	0.92	0.92
Infiltration	0.71	0.70	0.71	0.69	0.71	0.71
Mass	0.84	0.84	0.84	0.82	0.84	0.84
Nodule	0.78	0.76	0.77	0.72	0.77	0.78
Pleural T.	0.78	0.77	0.78	0.74	0.77	0.78
Pneumonia	0.76	0.76	0.75	0.72	0.78	0.77
Pneumothorax	0.86	0.87	0.87	0.84	0.86	0.86
Mean	0.83	0.83	0.83	0.80	0.83	0.85

Table 3: Areas under the receiver operating characteristic curves for the 14 chest pathologies. Training with OOD data does not affect chest X-ray classification performance. All models were tested on the CXR14 Wang et al. [2017] test set (ID).

To investigate the effect of training with OOD data on ID classification we measured the AUC on the test ID data set (CXR14). As shown in Table 3, training with OOD images did not affect ID classification performance, except when trained only with ImageNet.

References

- Varun Gulshan, Lily Peng, Marc Coram, Martin C. Stumpe, Derek Wu, Arunachalam Narayanaswamy, Subhashini Venugopalan, Kasumi Widner, Tom Madams, Jorge Cuadros, Ramasamy Kim, Rajiv Raman, Philip C. Nelson, Jessica L. Mega, and Dale R. Webster. Development and Validation of a Deep Learning Algorithm for Detection of Diabetic Retinopathy in Retinal Fundus Photographs. *JAMA*, 316(22):2402–2410, December 2016. ISSN 0098-7484. doi:10.1001/jama.2016.17216.
- Andre Esteva, Brett Kuperl, Roberto A. Novoa, Justin Ko, Susan M. Swetter, Helen M. Blau, and Sebastian Thrun. Dermatologist-level classification of skin cancer with deep neural networks. *Nature*, 542(7639):115–118, February 2017. ISSN 0028-0836, 1476-4687. doi:10.1038/nature21056.
- Pranav Rajpurkar, Jeremy Irvin, Kaylie Zhu, Brandon Yang, Hershel Mehta, Tony Duan, Daisy Ding, Aarti Bagul, Curtis Langlotz, and Katie Shpanskaya. Chexnet: Radiologist-level pneumonia detection on chest x-rays with deep learning. *arXiv preprint arXiv:1711.05225*, 2017.
- Pranav Rajpurkar, Jeremy Irvin, Robyn L. Ball, Kaylie Zhu, Brandon Yang, Hershel Mehta, Tony Duan, Daisy Ding, Aarti Bagul, Curtis P. Langlotz, Bhavik N. Patel, Kristen W. Yeom, Katie Shpanskaya, Francis G. Blankenberg, Jayne Seekins, Timothy J. Amrhein, David A. Mong, Safwan S. Halabi, Evan J. Zucker, Andrew Y. Ng, and Matthew P. Lungren. Deep learning for chest radiograph diagnosis: A retrospective comparison of the CheXNeXt algorithm to practicing radiologists. *PLOS Medicine*, 15(11):e1002686, November 2018a. ISSN 1549-1676. doi:10.1371/journal.pmed.1002686.
- Anna Majkowska, Sid Mittal, David F. Steiner, Joshua J. Reicher, Scott Mayer McKinney, Gavin E. Duggan, Krish Eswaran, Po-Hsuan Cameron Chen, Yun Liu, Sreenivasa Raju Kalidindi, Alexander Ding, Greg S. Corrado, Daniel Tse, and Shravya Shetty. Chest Radiograph Interpretation with Deep Learning Models: Assessment with Radiologist-adjudicated Reference Standards and Population-adjusted Evaluation. *Radiology*, 294(2):421–431, December 2019. ISSN 0033-8419. doi:10.1148/radiol.2019191293.
- Farah S. Ali, Samantha G. Harrington, Stephen B. Kennedy, and Sarwat Hussain. Diagnostic radiology in Liberia: A country report. *Journal of Global Radiology*, 1(2):6, 2015.
- Bukunmi Idowu and Tolulope Okedere. Diagnostic Radiology in Nigeria: A Country Report. *Journal of Global Radiology*, 6(1), June 2020. ISSN 2372-8418. doi:10.7191/jgr.2020.1072.
- David A. Rosman, Jean Jacques Nshizirungu, Emmanuel Rudakemwa, Crispin Moshi, Jean de Dieu Tuyisenge, Etienne Uwimana, and Louise Kalisa. Imaging in the land of 1000 hills: Rwanda radiology country report. *Journal of Global Radiology*, 1(1):5, 2015.
- Andrew B. Rosenkrantz, Danny R. Hughes, and Richard Duszak Jr. The US radiologist workforce: An analysis of temporal and geographic variation by using large national datasets. *Radiology*, 279(1):175–184, 2016.
- Abi Rimmer. Radiologist shortage leaves patient care at risk, warns royal college. *BMJ: British Medical Journal (Online)*, 359, 2017.
- Anh Nguyen, Jason Yosinski, and Jeff Clune. Deep Neural Networks Are Easily Fooled: High Confidence Predictions for Unrecognizable Images. In *Proceedings of the IEEE Conference on Computer Vision and Pattern Recognition*, pages 427–436, 2015.
- Eric Nalisnick, Akihiro Matsukawa, Yee Whye Teh, Dilan Gorur, and Balaji Lakshminarayanan. Do deep generative models know what they don’t know? In *International Conference on Learning Representations*, 2019.
- Dan Hendrycks, Kevin Zhao, Steven Basart, Jacob Steinhardt, and Dawn Song. Natural adversarial examples. In *Proceedings of the IEEE/CVF Conference on Computer Vision and Pattern Recognition*, pages 15262–15271, 2021.
- Paul Robinette, Ayanna M. Howard, and Alan R. Wagner. Effect of robot performance on human–robot trust in time-critical situations. *IEEE Transactions on Human-Machine Systems*, 47(4):425–436, 2017. doi:10.1109/THMS.2017.2648849.
- Effy Vayena, Alessandro Blasimme, and I Glenn Cohen. Machine learning in medicine: addressing ethical challenges. *PLoS medicine*, 15(11):e1002689, 2018.
- Oded Nov, Yindalon Aphinyanaphongs, Yvonne W Lui, Devin Mann, Maurizio Porfiri, Mark Riedl, John-Ross Rizzo, and Batia Wiesenfeld. The transformation of patient-clinician relationships with ai-based medical advice. *Communications of the ACM*, 64(3):46–48, 2021.
- Dan Hendrycks and Kevin Gimpel. A baseline for detecting misclassified and out-of-distribution examples in neural networks. In *ICLR*, 2017.
- Dan Hendrycks, Steven Basart, Mantas Mazeika, Mohammadreza Mostajabi, Jacob Steinhardt, and Dawn Song. Scaling Out-of-Distribution Detection for Real-World Settings. *arXiv:1911.11132 [cs]*, December 2020.

- Haoran Wang, Weitang Liu, Alex Bocchieri, and Yixuan Li. Can multi-label classification networks know what they don't know? *Advances in Neural Information Processing Systems*, 34, 2021.
- Dan Hendrycks, Mantas Mazeika, and Thomas Dietterich. Deep anomaly detection with outlier exposure. *ICLR*, 2019.
- Kimin Lee, Kibok Lee, Honglak Lee, and Jinwoo Shin. A simple unified framework for detecting out-of-distribution samples and adversarial attacks. *Advances in neural information processing systems*, 31, 2018.
- Alex Krizhevsky and Geoffrey Hinton. Learning multiple layers of features from tiny images. Technical report, University of Toronto, 2009.
- Yuval Netzer, Tao Wang, Adam Coates, Alessandro Bissacco, Bo Wu, and Andrew Y. Ng. Reading digits in natural images with unsupervised feature learning. In *NeurIPS Workshop on Deep Learning and Unsupervised Feature Learning*, 2011.
- Xiaosong Wang, Yifan Peng, Le Lu, Zhiyong Lu, Mohammadhadi Bagheri, and Ronald M. Summers. ChestX-ray8: Hospital-scale Chest X-ray Database and Benchmarks on Weakly-Supervised Classification and Localization of Common Thorax Diseases. In *2017 IEEE Conference on Computer Vision and Pattern Recognition (CVPR)*, pages 3462–3471, July 2017. doi:10.1109/CVPR.2017.369.
- Thomas Deserno and B. Ott. *15.363 IRMA Bilder in 193 Kategorien für ImageCLEFmed 2009*. 2009.
- Pranav Rajpurkar, Jeremy Irvin, Aarti Bagul, Daisy Ding, Tony Duan, Hershel Mehta, Brandon Yang, Kaylie Zhu, Dillon Laird, Robyn L. Ball, Curtis Langlotz, Katie Shpanskaya, Matthew P. Lungren, and Andrew Y. Ng. MURA: Large Dataset for Abnormality Detection in Musculoskeletal Radiographs. In *Medical Imaging with Deep Learning*, Amsterdam, 2018b.
- Safwan S. Halabi, Luciano M. Prevedello, Jayashree Kalpathy-Cramer, Artem B. Mamonov, Alexander Bilbily, Mark Cicero, Ian Pan, Lucas Araújo Pereira, Rafael Teixeira Sousa, Nitamar Abdala, Felipe Campos Kitamura, Hans H. Thodberg, Leon Chen, George Shih, Katherine Andriole, Marc D. Kohli, Bradley J. Erickson, and Adam E. Flanders. The RSNA Pediatric Bone Age Machine Learning Challenge. *Radiology*, 290(2):498–503, February 2019. ISSN 0033-8419. doi:10.1148/radiol.2018180736.
- Olga Russakovsky, Jia Deng, Hao Su, Jonathan Krause, Sanjeev Satheesh, Sean Ma, Zhiheng Huang, Andrej Karpathy, Aditya Khosla, Michael Bernstein, Alexander C. Berg, and Li Fei-Fei. ImageNet Large Scale Visual Recognition Challenge. *International Journal of Computer Vision*, 115(3):211–252, 2015.
- Antonio Torralba and Alexei A. Efros. Unbiased look at dataset bias. In *CVPR 2011*, pages 1521–1528, June 2011. doi:10.1109/CVPR.2011.5995347.
- Shiyu Liang, Yixuan Li, and R. Srikant. Enhancing the reliability of out-of-distribution image detection in neural networks. In *6th International Conference on Learning Representations, ICLR 2018*, 2018.
- Petra Bevandić, Ivan Krešo, Marin Oršić, and Siniša Šegvić. Simultaneous semantic segmentation and outlier detection in presence of domain shift. In *German Conference on Pattern Recognition*, pages 33–47. Springer, 2019.
- Gao Huang, Zhuang Liu, Laurens Van Der Maaten, and Kilian Q. Weinberger. Densely connected convolutional networks. In *Proceedings of the IEEE Conference on Computer Vision and Pattern Recognition*, pages 4700–4708, 2017.
- Diederik P. Kingma and Jimmy Ba. Adam: A Method for Stochastic Optimization. In *ICLR (Poster)*, 2015.